Solid State Phenomena
ISSN: 1662-9779, Vol. 358, pp 133-140
doi:10.4028/p-4Rj3jY

Submitted: 2023-10-02
Accepted: 2024-04-12
Online: 2024-08-21

Fast Estimation of the Lateral Fidelity of Ion Implantation in 4H-SiC through Calibration to JFET Transfer Characteristics in TCAD

K. Sakai[1,a*], N. Boettcher[2,b*], M. Szabo[2,c], S. Beuer[2,d], and M. Rommel[2,e]

[1]Institute of Industrial Science, The University of Tokyo, 4-6-1, Komaba Meguro-Ku, Tokyo 153-8505, Japan

[2]Fraunhofer Institute for Integrated Systems and Device Technology (IISB), 91058, Erlangen, Germany

[a]sakai@nano.iis.u-tokyo.ac.jp, [b]norman.boettcher@iisb.fraunhofer.de, [c]maximilian.szabo@iisb.fraunhofer.de, [d]susanne.beuer@iisb.fraunhofer.de, [e]mathias.rommel@iisb.fraunhofer.de

Keywords: 4H-SiC, Ion implantation, Lateral straggling, JFET, TCAD, Monte Carlo

Abstract. In the 4H-SiC device fabrication process, ion implantation of aluminium to form p-regions results in spreading (lateral straggling) from the mask design width by a few 100 nm. This has a significant impact on device performance, so device design must take lateral straggling into account. In this study, the impact of lateral straggling is estimated by applying a Gaussian distribution to one dimensional depth profiles obtained from Monte Carlo simulations. In our studies, this approach reduced the computation time by a factor of 300 compared to two-dimensional Monte Carlo simulations. The parameters describing the Gauss function are determined with the aid of fabricated JFET test structures. The pinch-off behaviour of JFET devices with vertical and horizontal channels was analysed in electrical TCAD simulations and calibrated to the characteristics of the fabricated devices. Ultimately, the electrical characteristics of simulations and measurements were found to be in good agreement.

Introduction

4H-SiC is being explored as a material for applications with operation at high temperatures or high voltages. In the SiC device fabrication process, mainly aluminium (Al) ion implantation is employed to create p-type regions of devices such as MOSFETs and JFETs. However, it is known that during Al ion implantation, the p-type region extends laterally over the mask edge by a few 100 nm [1, 2]. This lateral straggling has a significant impact on device operation, especially for devices containing JFET structures. Although, three-dimensional (3D) Monte Carlo (MC) simulation can accurately predict lateral straggling, the simulation itself is very time consuming [3]. Regarding the design process of device cells, the simulation effort becomes significant as, usually, multiple iterations of cell creation are employed to investigate the influence of a variation in cell geometry. Therefore, in this work, an accurate real-time estimation approach of the lateral straggling is proposed, which requires only a single one-dimensional (1D) MC simulation for any number of cell geometries.

Analytical

In this section, the theoretical equations for typical JFETs [4] are used to describe the relationship between channel width in 1st Epi ($a_{1\mathrm{st}}$), thickness of 2nd Epi ($a_{2\mathrm{nd}}$), and pinch-off operation of 2-channel JFETs as shown in Fig. 1 (b). In the following, depletion layer width (W_{d}), built-in potential (ψ_{BI}) and pinch-off (V_{P}) voltage for typical JFETs shown in Fig. 1 (a) are described, and then the pinch-off operation of 2-channel JFET is described. Assuming a single gate configuration and the source electrode to be grounded, W_{d} can be written as given in Eq. (1).

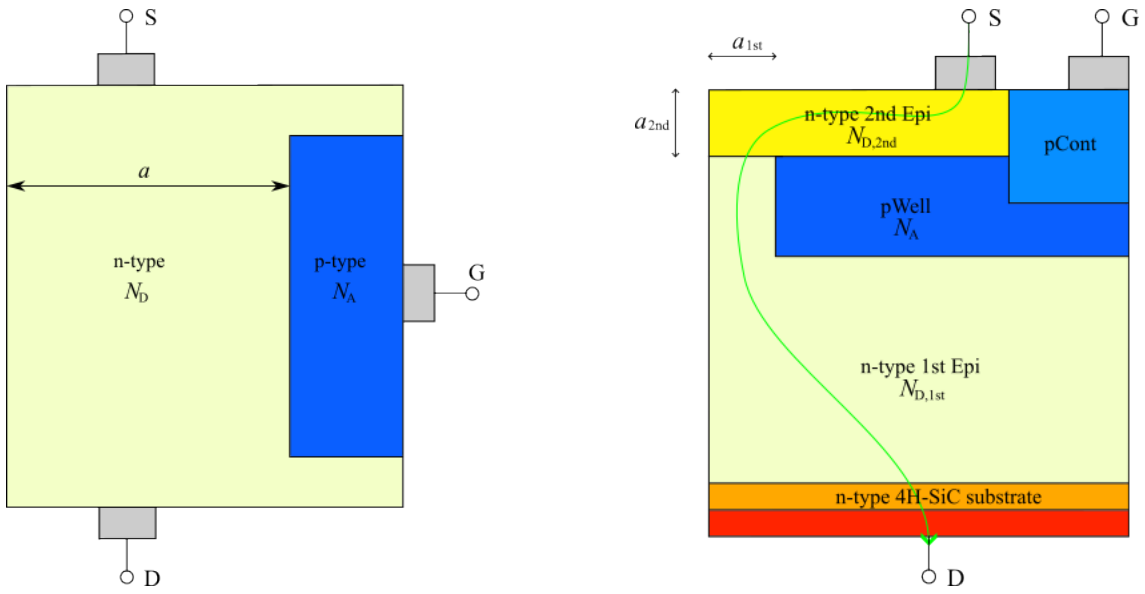

(a) (b)

Fig. 1. Schematic cross section of typical JFET(a) and the investigated JFET structure with vertical and horizontal channels(b). the green line illustrates the current path.

$$W_d = \sqrt{\frac{2\varepsilon_{SiC} N_A (\psi_{BI} - V_G)}{q N_D (N_A + N_D)}}, \tag{1}$$

where ε_{SiC} is the dielectric constant of 4H-SiC, V_G is the gate voltage, N_A is the acceptor concentration in the gate region, and N_D is the donator concentration in the channel region [4]. The built-in potential is given by

$$\psi_{BI} = \frac{kT}{q} \ln\left(\frac{N_A^- N_D^+}{n_i^2}\right), \tag{2}$$

where N_A^- and N_D^+ are the ionized doping concentrations in the gate and channel region, respectively [4]. In the transfer characteristic of an n-channel JFET, when a negative voltage is applied to the gate electrode, the depletion layer expands, closing the current path, eventually resulting in complete channel pinch-off. Hence, a specific value of V_G exists, where W_d is equal to half of the channel width (a), which is defined as pinch-off voltage (V_P). Thus, V_P can be written as

$$V_P = \psi_{BI} - \frac{q N_D (N_A + N_D) a^2}{2\varepsilon_{SiC} N_A}. \tag{3}$$

The fabricated JFET prototypes exhibit two channels as shown in Fig. 1 (b). Vertical and horizontal pn-junctions between pWell and 2nd Epi, as well as between pWell and 1st Epi are considered. The respective pinch-off voltages are expressed according to

$$V_{P,1st} = \psi_{BI,1st} - \frac{q N_{D,1st} (N_A + N_{D,1st}) a_{1st}^2}{2\varepsilon_{SiC} N_A} \tag{4}$$

and

$$V_{P,2nd} = \psi_{BI,2nd} - \frac{q N_{D,2nd} (N_A + N_{D,2nd}) a_{2nd}^2}{2\varepsilon_{SiC} N_A}. \tag{5}$$

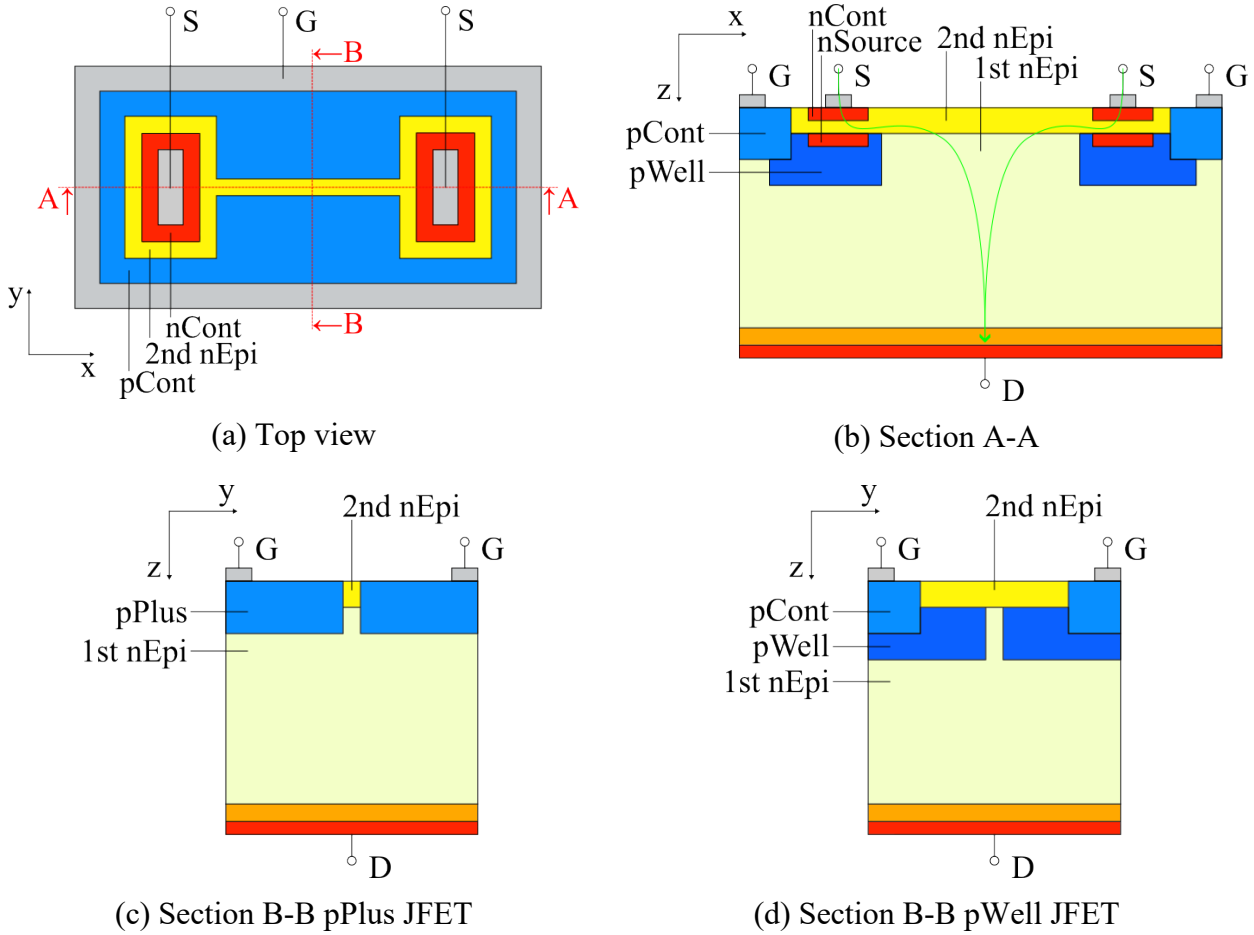

Fig. 2. Schematic top view (a) and cross-sectional views (b) to (d) of the fabricated devices. In (b), the green line illustrates the current path. In (c) and (d), the device variations pPlus and pWell are shown, respectively.

Here, a_{1st} is the channel width of the first channel, which is affected by lateral straggling and a_{2nd} is the channel width of the second channel determined by the thickness of the 2nd Epi layer. With respect to the investigation of lateral straggling, pinch-off in the second channel is rather undesired. To obtain pinch-off in the first channel, the condition $V_{P,1st} \leq V_{P,2nd}$ must be fulfilled. This leads to a critical value of a_{1st}, which is defined as a_{th}. Using Eq. (4) and Eq. (5) a_{th} is expressed as

$$a_{th} \leq \frac{N_{D,2nd}\left(N_A + N_{D,2nd}\right)a_{2nd}^2}{N_{D,1st}\left(N_A + N_{D,1st}\right)} - \frac{2\varepsilon_{SiC}N_A kT}{q^2}\ln\left(\frac{N_{D,2nd}^+}{N_{D,1st}^+}\right). \tag{6}$$

Consequently, values of $a_{1st} > a_{th}$ have no influence on the pinch-off operation of the full device. From Eq. (6), the effective pinch-off voltage $V_{P,eff}$ can be determined to

$$V_{P,eff} = \begin{cases} V_{P,1st}\ (a_{1st} < a_{th}) \\ V_{P,2nd}\ (a_{1st} > a_{th}) \end{cases}. \tag{7}$$

Fabrication

For verification, the lateral straggling is calibrated to experimental results of the transfer characteristics of vertical 4H-SiC JFET devices shown in Fig. 2. The devices were fabricated using an existing 4H-SiC JFET process technology, which is based on the utilization of two epitaxial layers

Table 1. Ion implantation energies and doses for pPlus and pWell structures.

Implantation	pWell		pPlus	
	Energy (keV)	Dose (cm^{-2})	Energy (keV)	Dose (cm^{-2})
1	540	4.00E+13	540	1.20E+14
2	220	1.00E+12	380	7.60E+13
3	140	1.00E+12	245	6.00E+13
4	75	7.00E+12	115	4.80E+14
5	35	4.00E+12	60	2.00E+14
6			30	1.20E+14

(1st Epi and 2nd Epi) [5, 6]. The JFET channel structures are created in two variations employing Al ion implantation for the p-type doping profiles of pPlus and pWell. The ion implantation energies and doses that comprise the pWell and pPlus doping profiles are shown in Table 1. The angle of ion implantation was 7 °. In the fabricated devices, the current flows horizontally in the 2nd Epi and, subsequently, vertically in the 1st Epi from the drain (D) electrode to the source (S) electrode. Applying a negative voltage to the gate (G) electrode causes the depletion layer to expand from the pn-junctions, narrowing the channel region and, ultimately, blocking the current. Therefore, the transfer characteristics are strongly determined by the channel width. Fig. 3 shows SEM images of cross sections of the fabricated JFET structures, which were created with the help of focused ion beam. It is known that in 4H-SiC SE Potential Contrast significantly depends on doping concentration and doping type for properly chosen SEM imaging parameters [5]. As can be observed, the doped regions significantly extend over the mask edge, narrowing the effective channel width.

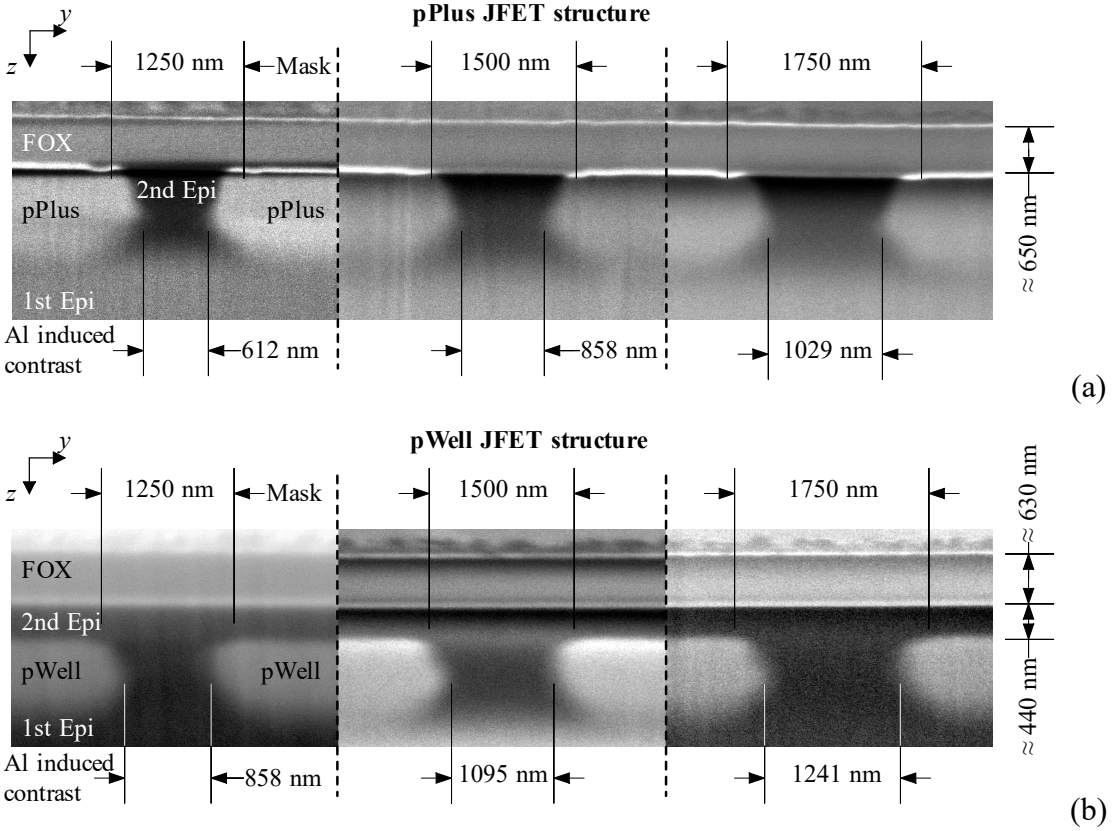

Fig. 3. Cross-sectional SEM images of the fabricated pPlus (a) and pWell (b) structures.

Modeling of the 3D Doping Profiles

1D MC simulation results of the pPlus and pWell profiles in *z*-direction are shown in Fig. 4 (a) emphasizing the difference in doping concentration and depth. For the proposed method, these

z-directed 1D profiles are applied to a polygon in the xy-plane to obtain 3D doping profiles, which are homogeneous within the geometrical boundaries of the polygon. In the model, the lateral straggling beyond these boundaries is assumed to follow a Gaussian distribution, according Eq. (8). The extent of straggling ($\mathrm{N_{A,y}}$) is determined by the doping concentration at a certain depth ($\mathrm{N_{A,z}}(z)$) and the calibration parameter (y_{Gauss}), which indicates a decrease of $\mathrm{N_{A,y}}$ to $\mathrm{N_{A,z}}(z) \cdot \exp(-1)$. For reference, the result of Eq. (8) for $y_{\mathrm{Gauss}} = 200$ nm normalized to $\mathrm{N_{A,z}}(z)$ is plotted in Fig. 4 (b).

$$N_{\mathrm{A,y}}(y,z) = N_{\mathrm{A,z}}(z) \cdot \exp\left(-\left[\frac{y}{y_{\mathrm{Gauss}}}\right]^2\right) \tag{8}$$

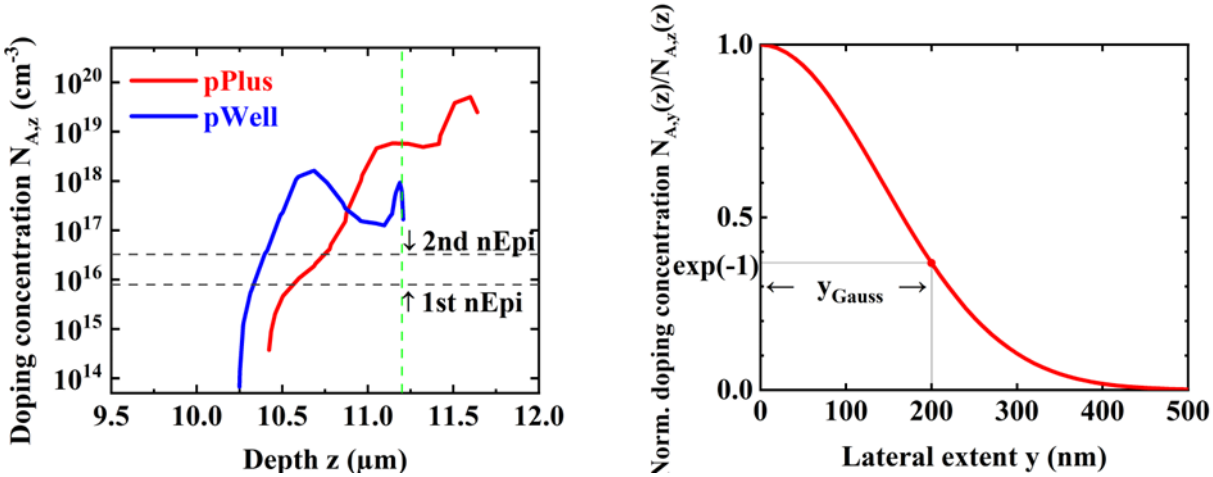

Fig. 4. Monte Carlo simulation results of the doping profiles in the z-direction (a) and Gaussian distribution of the lateral straggling in y-direction for $y_{\mathrm{Gauss}} = 200$ nm (b). In (a), the green dotted line represents the boundary between the 1st and 2nd Epi. The lateral distribution in x-direction is identical to the y-direction shown in (b).

To compare the proposed method to a conventional simulation, a 2D MC simulation of the structure depicted in Fig. 3 is performed. Fig. 6 shows the active aluminum concentration according to the 2D MC implantation and the proposed approach (1D MC + Gauss) in case of the pPlus structure. The qualitative shape of the 2D MC pPlus implantation matches the shape that can be observed in Fig. 3 (a). In contrast, the calibrated Gaussian profile is not showing the distinct bulge shape since the extent of lateral straggling is proportional to the doping concentration at a certain depth. Hence, a pronounced straggling close to the surface is observed in case of the pPlus profile. Notably, the proposed method aims for a good match of the electrical characteristics rather than to result in an exact representation of the lateral shape of the implantation profile as is demonstrated later.

As shown in Fig. 7, both methods yield to results, which qualitatively are in good agreement with the SEM images depicted in Fig. 3 (b). In case of pWell, the highest doping concentration is obtained at a depth of approximately 1 µm measured from the 1st Epi surface. A result, a bulgy lateral shape is gained from the proposed method as depicted in Fig. 7 (b). The beak close to the 1st Epi surface occurs due to the high surface doping concentration of the pWell profile as discussed above.

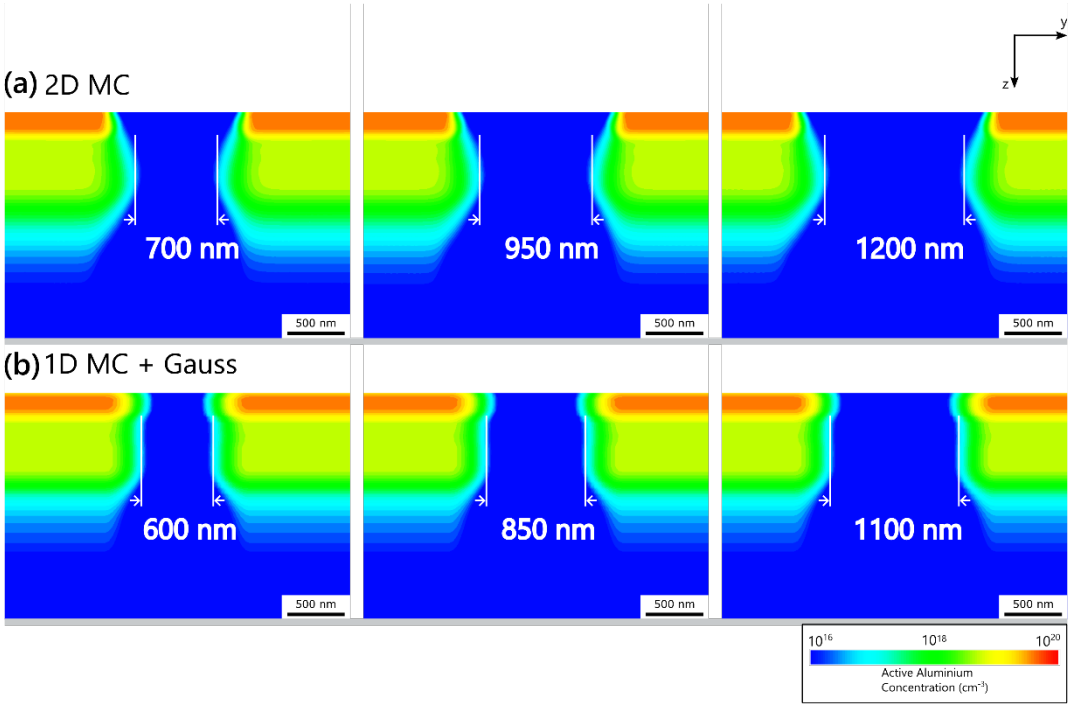

Fig. 6. 2D Simulation of the devices depicted in Fig. 3 (a) using 2D Monte Carlo simulation (a) and the 1D Monte Carlo pPlus profile combined with the adapted Gaussian distribution of the lateral straggling in *y*-direction (b).

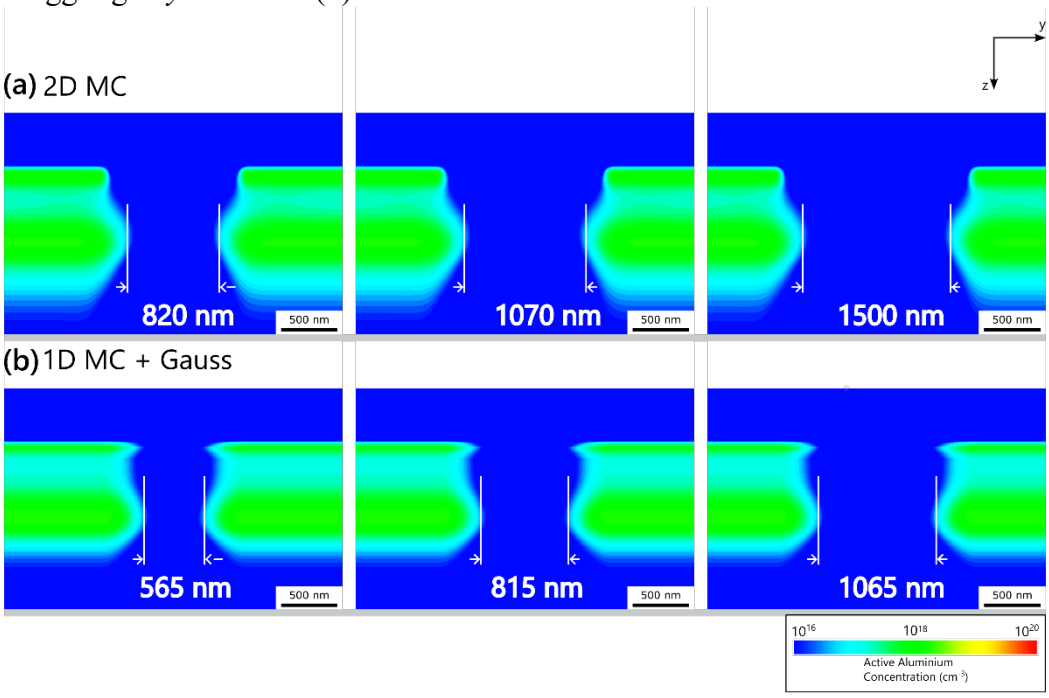

Fig. 7. 2D Simulation of the devices depicted in Fig. 3 (b). Using 2D Monte Carlo simulation (a) and the 1D Monte Carlo pWell profile combined with the adapted Gaussian distribution of the lateral straggling in *y*-direction (b).

For both the pPlus and the pWell implantation, the calibrated Gaussian underestimate the depth of the implantation. This is likely caused by channeling effects, which cannot be considered by 1D MC simulation. Moreover, the proposed method cannot account for a difference in the left or right side of the implantation shape caused by the 4° off-axis of the SiC wafers. As can be obtained from Fig. 2 (a), the channel stripes were arranged along the x-axis, which corresponds to the $[11\bar{2}0]$ crystal direction. Therefore, the channel width is affected by the lateral straggling in the $[1\bar{1}00]$ direction. Lateral straggling in the $[1\bar{1}00]$ direction is reported to be more symmetrical than in the $[11\bar{2}0]$ direction [1, 2].

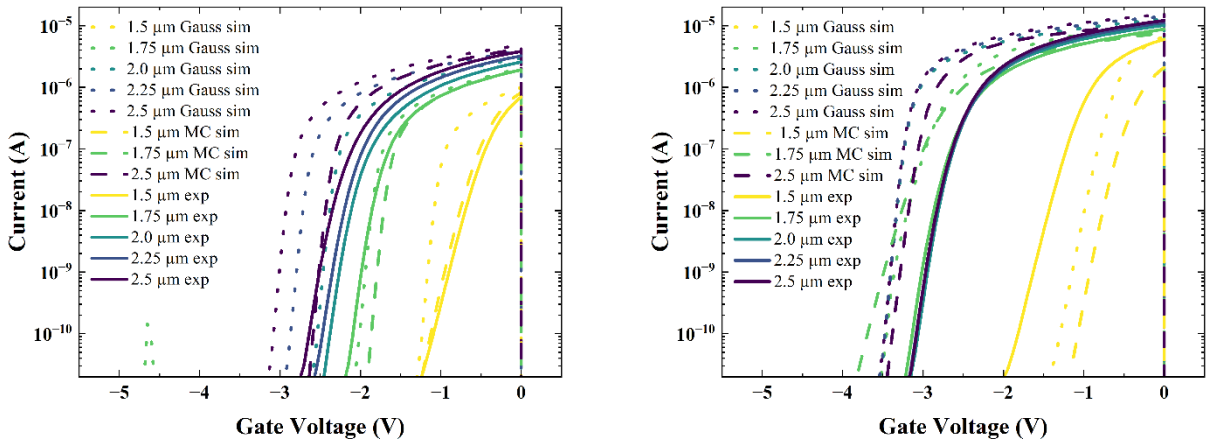

Fig. 5. Transfer characteristics of the pPlus (a) and pWell (b) JFET structures with various channel widths. The dotted and solid lines represent simulation results with optimized values of y_{Gauss} and $N_{\mathrm{D,2nd}}$ and measurement results, respectively.

Nevertheless, the computation time required for the calibrated Gaussian simulation approach for all depicted profiles is 90 sec and approximately 80 min excluding and including the preceding 1D MC simulation. In comparison, the 2D MC simulation for all depicted profiles takes 7.5 h. Notably, when performing a parameter study to e.g., optimize the design parameters of a device cell, the 1D MC simulation is to be performed only once, whereas the 2D MC must be repeated for each design. Thus, the absolute computation time is reduced by a factor of 300 for each design iteration using the proposed approach.

Calibration Result

In the following, the Gaussian parameter (y_{Gauss}) and the doping concentration of the 2nd Epi layer ($N_{\mathrm{D,2nd}}$) and are optimized to calibrate the model to the measured pinch-off characteristics in the 1st and the 2nd Epi, respectively. In Fig. 5, the transfer characteristics obtained from electrical measurements in comparison to the calibrated TCAD simulation results for the JFET structures shown in Fig. 2 (c) and (d) are presented. For the calibration, y_{Gauss} for pPlus and pWell are determined to 85 nm and 90 nm, respectively. As can be observed in case of the pWell structure, for a channel width of 2 µm or longer, the pinch-off voltage saturates at approximately 3.5 V. This is explained by the rather parasitic effect of vertical pinch-off in the 2nd Epi layer. Nevertheless, both the simulation results of the pinch-off in the 1st Epi layer as well as in the 2nd Epi layer are in good agreement with the experiments.

Conclusion

In this study, a refined approach to estimate the impact of lateral straggling in Al ion implantation into 4H-SiC on device performance is proposed, which applies a lateral Gaussian distribution to 1D Monte Carlo doping profiles. A comparison of the calibrated Gaussian to a 2D MC simulation shows that although the proposed approach cannot account for 2D channeling effects and the difference in shape of the left and right side implantation caused by 4° off-axis, the simulation results were found to be in good agreement with the transfer characteristics of fabricated 4H-SiC JFETs. It is worth mentioning, that the determined values of the optimisation parameters may not be valid for doping profiles other than the investigated. Nevertheless, the determined values of 85 nm and 90 nm for the pWell and pPlus structures, respectively, are reasonably close to each other to expect good results by using them for simulations of comparable doping profiles. Furthermore, the benefit gained from this approach in terms of computing time allows for a considerable increase in flexibility during the design

phase of devices. Therefore, we believe, that the findings of this study pose a valuable contribution to the development of 4H-SiC electronic devices.

References

[1] J. Müting, et al. *Applied Physics Letters* 116, no. 1 (2020): 012101.

[2] Q. Jin, et al. *Japanese Journal of Applied Physics* 60, no. 5 (2021): 051001.

[3] P. Pichler, et al. *Materials Science Forum* 963, (2019): 386–89.

[4] T. Kimoto and J. Cooper. *Unipolar Power Switching Devices. Fundamentals Of Silicon Carbide Technology: Growth, Characterization, Devices And Applications*, (2014): 301-352.

[5] M. Buzzo, M. Ciappa, M. Stangoni, W. Fichtner, *Microelectronics Reliability*, Volume 45, Issues 9–11, 2005, Pages 1499-1504, doi.org/10.1016/j.microrel.2005.07.069.